

Homogeneous and heterogeneous ice nucleation at LACIS: operating principle and theoretical studies

S. Hartmann¹, D. Niedermeier¹, J. Voigtländer¹, T. Clauss¹, R. A. Shaw^{1,2}, H. Wex¹, A. Kiselev^{1,3}, and F. Stratmann¹

¹Leibniz Institute for Tropospheric Research, Department of Physics, 04318 Leipzig, Germany

²Michigan Technological University, Department of Physics, Houghton, Michigan 49931, USA

³Karlsruhe Institute of Technology, Institute for Meteorology and Climate Research Atmospheric Aerosol Research Department, 76344 Eggenstein-Leopoldshafen, Germany

Received: 18 October 2010 – Published in Atmos. Chem. Phys. Discuss.: 1 November 2010

Revised: 16 February 2011 – Accepted: 17 February 2011 – Published: 25 February 2011

Abstract. At the Leipzig Aerosol Cloud Interaction Simulator (LACIS) experiments investigating homogeneous and heterogeneous nucleation of ice (particularly immersion freezing in the latter case) have been carried out. Here both the physical LACIS setup and the numerical model developed to design experiments at LACIS and interpret their results are presented in detail.

Combining results from the numerical model with experimental data, it was found that for the experimental parameter space considered, classical homogeneous ice nucleation theory is able to predict the freezing behavior of highly diluted ammonium sulfate solution droplets, while classical heterogeneous ice nucleation theory, together with the assumption of a constant contact angle, fails to predict the immersion freezing behavior of surrogate mineral dust particles (Arizona Test Dust, ATD). The main reason for this failure is the compared to experimental data apparently overly strong temperature dependence of the nucleation rate coefficient.

Assuming, in the numerical model, Classical Nucleation Theory (CNT) for homogeneous ice nucleation and a CNT-based parameterization for the nucleation rate coefficient in the immersion freezing mode, recently published by our group, it was found that even for a relatively effective ice nucleating agent such as pure ATD, there is a temperature range where homogeneous ice nucleation is dominant. The main explanation is the apparently different temperature dependencies of the two freezing mechanisms. Finally, reviewing the assumptions made during the derivation of the CNT-

based parameterization for immersion freezing, it was found that the assumption of constant temperature during ice nucleation and the chosen ice nucleation time were justified, underlining the applicability of the method to determine the fitting coefficients in the parameterization equation.

1 Introduction

Ice containing clouds have an impact on the Earth's radiative balance by scattering and absorbing solar and terrestrial radiation (Zuberi et al., 2002; Hung et al., 2003). Ice formation in clouds changes cloud radiative properties (DeMott et al., 2003b), affects cloud dynamics, chemical processes, charge separation in cumulonimbus clouds (Takahashi, 1978), and is the source of effective pathways to form precipitation in mixed-phase clouds. Therefore, ice formation processes greatly impact cloud lifetime and Earth's climate (Lohmann, 2006).

Ice formation in the atmosphere takes place via homogeneous and heterogeneous ice nucleation processes. Homogeneous ice nucleation proceeds from a stochastic event in liquid water or aqueous solution droplets without being catalyzed by a foreign substance. In contrast heterogeneous ice nucleation is induced by foreign substances called ice forming nuclei (IN) (Cantrell and Heymsfield, 2005). In general four different heterogeneous freezing modes are distinguished: deposition nucleation, condensation, immersion and contact freezing mode (e.g., Pruppacher and Klett, 1997). In the framework of the present paper, we will mainly concentrate on immersion freezing being defined as: A partly



Correspondence to: S. Hartmann
(hartmann@tropos.de)

insoluble aerosol particle acts initially as cloud condensation nucleus (CCN) or becomes immersed after collision in a droplet. Due to temperature decrease, ice nucleation takes place directly at the IN surface and induces the freezing of the supercooled droplet.

In general, the understanding of the physical and chemical processes underlying heterogeneous ice formation is limited. Therefore, more scientific work, both theoretical and experimental, is necessary to elucidate fundamental physical and chemical mechanisms, as well as to develop adequate parameterizations that are suitable for use in cloud and global models (Kärcher and Lohmann, 2003; Cantrell and Heymsfield, 2005).

Various field observations of droplet freezing through heterogeneous ice nucleation show that insoluble substances, especially mineral dust particles, act as IN in the atmosphere (DeMott et al., 2003a,b; Sassen et al., 2003; Cziczo et al., 2004; Richardson et al., 2007; Seifert et al., 2010). Mineral dust particles originate from desert and arid regions and can be lifted into the free troposphere during storm events. Subsequently, the dust particles can be transported over large distances (Prospero, 1999; Sassen et al., 2003; DeMott et al., 2003a). As a result mineral dust particles indirectly influence cloud properties, precipitation, and therefore Earth's climate (Zuberi et al., 2002; DeMott et al., 2003a,b).

Considering laboratory studies, there are numerous methods for investigating homogeneous and heterogeneous ice nucleation. Examples are wind tunnel experiments (Pruppacher and Neiburger, 1968; Diehl and Mitra, 1998), the method of electrodynamic droplet levitation (Davis, 1997; Duft and Leisner, 2004), differential scanning calorimetry (Koop et al., 1999; Chang et al., 1999), optical microscopy in a cold stage cell (Koop et al., 1998; Murray et al., 2010) and cloud chamber methods. Concerning the latter, three different types of cloud chambers are classified according to the mechanism used to achieve supersaturation with respect to water and/or ice. Supersaturation with respect to water and ice can be obtained by adiabatically expanding the gas inside the chamber (expansion cloud chamber, e.g. Aerosol Interaction and Dynamics in the Atmosphere (AIDA, Möhler et al., 2003), using the mixing of warm humidified with cold dry air (e.g. Fast Ice Nucleus CHamber FINCH, Bundke et al., 2008), or by combined heat-vapor diffusion (diffusion cloud chamber, e.g. the Leipzig Aerosol Cloud Interaction Simulator (LACIS), Stratmann et al. (2004), the Continuous Flow thermal gradient Diffusion Chamber (CFDC), Rogers, 1988 and Zurich Ice Nucleation Chamber (ZINC), Stetzer et al., 2008).

During the measurement campaign FROST (FReezing Of duST), which took place in April 2008 at the Leibniz Institute of Tropospheric Research (IfT), the ability of mineral dust particles (Arizona Test Dust, ATD) to function as IN was investigated and quantified at the laminar flow diffusion cloud chamber LACIS (Niedermeier et al., 2010). The aerosol particles used were characterized with respect to shape, chemi-

cal composition, hygroscopic growth and droplet activation. During an immersion freezing experiment performed with LACIS the water droplets were dispersed in air. It should be noted that each droplet contained just one particle/IN, with the particles all possessing approximately the same size. In order to quantify the immersion freezing behavior, fractions of frozen droplets as a function of temperature were determined over a temperature range from 233.15 K to 240.65 K. Based on these measurements, a parameterization of the ice nucleation rate describing the immersion freezing of ATD particles was derived.

The three main foci of the present paper are the description of (1) the physical setup and operating principle of LACIS for investigating homogeneous and heterogeneous ice nucleation (especially immersion freezing in the latter case), (2) the introduction of the numerical model developed to design and interpret the experiments at LACIS, and (3) the interpretation of actual experimental results by comparing with ice nucleation theory (Classical Nucleation Theory and a CNT-based parameterization). This rather theoretical paper and that of Niedermeier et al. (2010) are linked closely. In Niedermeier et al. (2010) mainly the experimental results are presented, whereas in this paper for the first time, the numerical model FLUENT/FPM (Computational Fluid Dynamics (CFD) code FLUENT, Fluent Inc., 2001) combined with the Fine Particle Model (FPM, Particle Dynamics GmbH, Wilck et al., 2002; Whitby et al., 2003) is introduced, as extended version to deal with ice nucleation. The coupled fluid and particle dynamical processes taking place in LACIS are illustrated including the presentation of the temperature, supersaturation, droplet/ice particle mass fraction, and nucleation rate profiles. As extended, the numerical model accounts for both, homogeneous and heterogeneous ice nucleation separately. Furthermore, the validity of assumptions made for the CNT-based parameterization of immersion freezing in Niedermeier et al. (2010) is discussed.

2 Leipzig Aerosol Cloud Interaction Simulator for ice nucleation

The laminar flow diffusion cloud chamber LACIS was constructed to investigate cloud microphysical processes like hygroscopic growth and droplet activation of aerosol particles under atmospherically relevant conditions (Stratmann et al., 2004). Basically, LACIS is a laminar flow tube of adjustable length consisting of a variable number of 1 m long tube segments (also called sections). For studying homogeneous and heterogeneous ice nucleation, LACIS was extended to its full length of 7 m by adding sections covering the supercooling temperature range $T < T_0 = 273.15$ K, where ice nucleation can occur. The residence times inside this long version of LACIS range from about 2 to 50 s. The temperature can be varied from 298 down to 223 K under operational pressures from 700 hPa to ambient values.

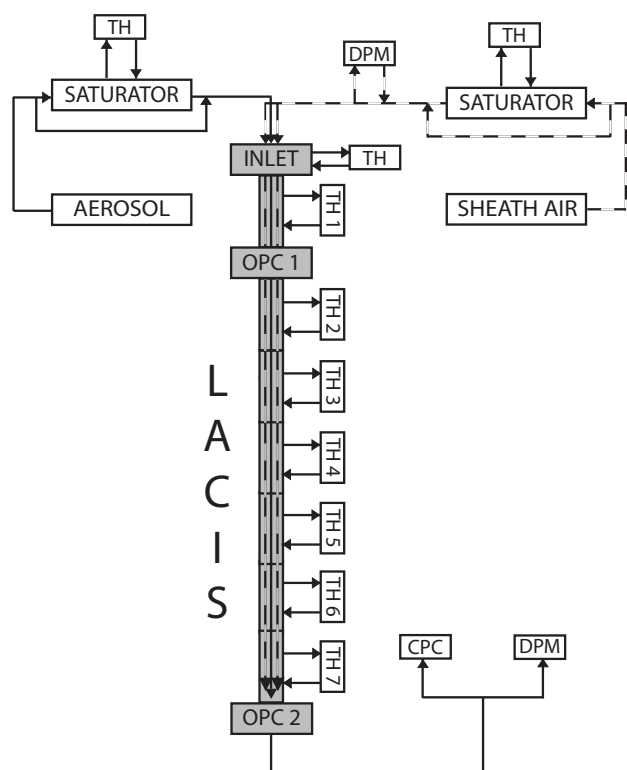


Fig. 1. Schematic of LACIS setup with conditioning part, cloud chamber/laminar flow tube and detection system (OPC 1 and OPC 2). The abbreviation TH means thermostat, DPM represents chilled mirror dew point hygrometer, CPC depicts the condensational particle counter and OPC stands for optical particle counter.

Inside LACIS supersaturations with respect to water and/or ice are achieved by a combined heat and vapor diffusion process. For determining suitable experimental conditions and quantitative interpretation of experimental data, the numerical model FLUENT/FPM-FLUENT in combination with the Fine Particle Model developed at IfT is applied.

LACIS as a whole consists of a flow conditioning system, the laminar flow tube itself, and optical particle detectors systems. A schematic of the LACIS instrument setup is given in Fig. 1.

2.1 Aerosol particle generation and conditioning

The aerosol flow is generated by dispersing various different aerosol particles (e.g. mineral dust, soot, ammonium sulfate particles) in a particle free air flow. Different coating devices are available for modifying the aerosol particles' surfaces by applying coatings of different atmospherically relevant chemical substances (e.g. sulfuric acid, ammonium sulfate, succinic acid, see Stratmann et al., 2004; Niedermeier et al., 2010). In order to enable size-resolved examination of the aerosol particles, a Differential Mobility Analyzer (DMA, type Vienna Medium, Knutson and Whitby, 1975; Reischl,

1991) is utilized, which selects quasi-monodisperse particles according to their electrical mobility.

In addition to the aerosol flow a particle free sheath air flow controlled by a mass flow controller (MFC 1179, MKS, Andover, MA) is provided. Both flows are conditioned with respect to temperature and humidity prior entering the flow tube (Fig. 1). Therefore both flows are humidified to defined dew point temperatures by two separate saturators (aerosol: MH-110-12S-4, sheath air: PH-30T-24KS, Perma Pur, Toms River, New Jersey). The saturators consist of semipermeable Nafion[®] tubes surrounded by water jackets, which are temperature controlled by the respective thermostats (TH, aerosol air: F25, sheath air: FP50, Julabo, Seelbach, Germany). The saturator of the aerosol air flow can also be bypassed, so that the aerosol flow remains dry ($T_d \approx 233$ K). The inlet dew point temperatures of the sheath air flow can be varied in the range between 233 and 293 K by mixing humidified and dry air flows. An inline-connected chilled mirror dew point hygrometer (DPM, DewMaster, EdgeTech, Marlborough, MA) monitors the dew point temperature of the sheath air flow. The aerosol and sheath air flows are combined in the inlet section of LACIS. The inlet serves as heat exchanger (temperature controlled by a thermostat with an accuracy of 0.01 K, TH, F25, Julabo, Seelbach, Germany) for harmonizing the temperatures of both air flows and combining them at the entrance of the laminar flow tube. At this point, initial condition such as inlet temperature T_{IN} , inlet dew point temperature $T_{d,IN}$ and flow velocities \bar{u} , are well defined and known for consideration in experimental data interpretation and for use in the numerical model.

2.2 Laminar flow tube

The sheath air enters the laminar flow tube isokinetically with the aerosol flow, with the latter forming an approximately 2-mm-diameter aerosol beam at the flow tube center. The volume flow rates of aerosol and sheath air are 0.081 min^{-1} and 4.001 min^{-1} respectively, (corresponding to a mean flow velocity of $\bar{u} = 0.4 \text{ m s}^{-1}$) with the first being adjusted by a mass flow controller (MFC 1179, MKS, Andover, MA) at the LACIS outlet.

The newly developed long version of the laminar diffusion cloud chamber LACIS (Fig. 1) consists of seven linked one-meter tube sections with an inner diameter of 15 mm. The wall temperatures of the seven tube sections are adjusted separately by thermostats (TH, Sect. 1–5: FP50, Sect. 6–7: LH85, Julabo, Seelbach, Germany). The temperature control of the tube walls follows the counter flow principle, i.e., the cooling fluids run in the reverse direction compared to the flow inside the tube. In order to control and monitor these wall temperatures, external resistance thermometers (Pt100, B 1/10 pursuant DIN EN 60751, additional calibration at IfT) are used to control the refrigerant temperatures in the supply (the thermometers are connected to the thermostats' control circuits) and measure them in the return line of the cooling

Table 1. LACIS operating parameters.

Flow tube length, L	7.0 m
Flow tube diameter, D	15.0 mm
Tube wall material	stainless steel
Operating pressure, p	700 hPa – ambient pressure
Average inlet velocity, \bar{u}_{IN}	$0.1\text{--}0.5\text{ m s}^{-1}/0.4\text{ m s}^{-1}$
Particle number concentration, N_p	$\approx 300\text{ \# cm}^{-3}$
Mean inlet particle diameter (dry), d_p	e.g. 200, 300 nm
Initial particle material	e.g. $(\text{NH}_4)_2\text{SO}_4$, ATD
Inlet temperature, T_{IN}	293.15 K
Inlet dew point, $T_{d,IN}$	293.05 to 233.15 K
Wall temperature of Sect. 1, $T_{w,1}$	293.15 to 273.15 K
Wall temperature of Sect. 2, $T_{w,2}$	293.15 to 258.15 K
Wall temperature of Sect. 3, $T_{w,3}$	273.15 to 258.15 K
Wall temperature of Sect. 4, $T_{w,4}$	273.15 to 258.15 K
Wall temperature of Sect. 5, $T_{w,5}$	273.15 to 258.15 K
Wall temperature of Sect. 6, $T_{w,6}$	273.15 to 233.15 K
Wall temperature of Sect. 7, $T_{w,7}$	273.15 to 233.15 K

cycle of each tube section. With this configuration a wall temperature accuracy of 0.10 K with a stability of ± 0.01 K for section 1 to 5 and for the last two tube sections an accuracy of 0.30 K with a stability of ± 0.10 K is attained. The wall temperature error of 0.3 K is derived from the temperature fluctuation of the water jacket refrigerant enveloping a tube section due to temperature regulation of the respective thermostat. The flow tube is vertically oriented and operated in a top to bottom flow direction. The flow inside the tube is laminar and axisymmetric with a stable, well-defined aerosol particle beam at the center of the flow tube (Stratmann et al., 2004). The operating parameters of LACIS are summarized in Table 1.

Downstream of the laminar flow tube, a Condensation Particle Counter (CPC 3010, TSI Inc., St. Paul, Minnesota, USA), operating at 1.01 min^{-1} , is used to measure the aerosol particle number concentration, and a Dew Point Mirror (DPM 973, MBW Calibration Ltd., Wettingen, Switzerland), operating at 0.71 min^{-1} , monitors the outlet dew and frost point temperatures.

2.3 Particle detection

To detect seed particles, water droplets, and ice particles, two different Optical Particle Counters (OPC) are installed at the LACIS setup. The upper white-light optical particle spectrometer (OPC 1 in Fig. 1, described in Kiselev et al., 2005), which is situated between tube sections 1 and 2, is used to analyze the size distribution of the aerosol particles and/or water droplets after passing the first tube section. It was not used in the experiments dealt with here, but is mentioned for completeness. At the outlet of LACIS, the white light aerosol spectrometer (WELAS[®] 1000, Palas GmbH, Karlsruhe, Germany, OPC 2 in Fig. 1) was used during the FROST measurement campaign. When measuring with the WELAS instrument the differentiation between frozen

droplets and seed particles, that is needed to determine ice fractions, was realized via evaluation of the measured size distributions (Niedermeier et al., 2010). In order to distinguish directly between ice particles and water droplets/seed particles having identical sizes (via phase state and therefore surface structure), two further optical devices applying different techniques can be employed in future applications: (i) the Thermostabilized Optical Particle Spectrometer (TOPS-ICE, developed at IfT), which allows to distinguish between spherical (droplets) and non-spherical (seeds and ice particles) particles by detecting the polarization state of the scattered light and (ii) the LISA instrument (Lacis Ice Scattering Apparatus, University of Hertfordshire, Hatfield AL10 9AB, United Kingdom, Hirst et al., 2001), with which two-dimensional diffraction scattering patterns of the investigated particles are recorded.

2.4 Applications and modes of operation

For investigating hygroscopic growth, activation, and heterogeneous ice nucleation behavior of size-segregated well-defined aerosol particles, LACIS can be operated in different modes which depend on the actual boundary conditions. These are the water sub- and supersaturated modes for the temperature range above $T_0 = 273.15$ K, the water sub-, ice supersaturated, and the water super- and ice supersaturated modes below $T_0 = 273.15$ K. If the inlet dew point temperature is lower than the wall temperature, the inner tube walls are in equilibrium with the water vapor of the flow and the dew point temperature remains constant (water sub-saturated mode). Applying this water sub-saturated mode for $T > 273.15$ K with inlet and wall temperature being identical, deliquescence and hygroscopic growth of aerosol particles can be investigated (Wex et al., 2006, 2007; Voigtländer et al., 2008; Ziese et al., 2008; Niedermeier et al., 2008). With higher inlet dew point temperature compared to the wall temperature, supersaturation can be achieved as a result of the simultaneous heat and vapor diffusion, which occur at slightly different rates, because of the non-linearity of the water vapor pressure curve. In this mode, the water vapor condenses on both the aerosol particles and the inner tube walls. As a result a thin water film accumulates on the tube walls and the dew point temperature of the flow converges to the wall-temperature set point. With this method, critical supersaturations for cloud droplet activation and growth, including kinetic effects, can be studied (Wex et al., 2006, 2007; Voigtländer et al., 2008; Niedermeier et al., 2008; Ziese et al., 2008).

Homogeneous and heterogeneous ice nucleation processes can be investigated with LACIS. In particular for heterogeneous ice nucleation two different freezing modes can be studied: immersion freezing and deposition nucleation. In order to analyze deposition nucleation, LACIS can be operated in the water subsaturated and ice supersaturated mode at temperatures below 273.15 K. In this study, we mainly

concentrate on water supersaturated conditions to study homogeneous and, especially, immersion freezing processes. A simple and straight forward mode of operation was used for LACIS, i.e., following Niedermeier et al. (2010), sections 6 and 7 were applied to activate the seed particles to water droplets and subsequently freeze them by further temperature decrease. Other modes are possible but not dealt with here. To achieve reproducible and well-defined measurement conditions, it is ensured that a thin ice layer covers the inner tube walls. This is realized by accumulating liquid water on the tube walls which is then converted to ice by cooling the walls down below 233 K.

It should be noted, that both model calculations (see below) and experiments are carried out assuming steady state conditions. In other words, boundary conditions are held constant in both model and experiment. However, the building up of the ice layer on the tube walls may introduce an undesired transient behavior. The initial ice layer is generated before each experiment and slowly grows during the experiment. Possible effects of the ice growth are (1) an increased flow velocity inside LACIS, (2) time dependent heat transfer to the tube walls, (3) a disturbance of the laminar flow profile, and (4) the splintering of small ice crystals from the ice layer. Effects (1) and (2) are observed for longer measurement times, and experiments are stopped as soon as they become noticeable. Furthermore, experiments are repeated multiple times, performed in different sequences of the different wall temperature settings, and show similar results. Disturbances of the laminar flow profile (3) influence the stability of the aerosol beam at the center of LACIS. This effect is directly observable in the optical particle counter underneath LACIS but occurs much later than effects (1) and (2), i.e. measurements are usually terminated before this effect occurs. Towards the end of a measurement it can appear that ice crystal parts break off the ice layer covering the wall inside LACIS (4). For these differently sized and oriented ice particles the scattering signals at the OPC could be discerned from those of desired particles so that an exact determination of the ice fraction is possible. However, as soon as this effect occurs the experiment is stopped. In summary, experiments are terminated as soon as transient effects start to occur.

3 Numerical model and nucleation rate coefficients

3.1 Numerical model

The numerical model is able to simulate the hygroscopic growth of the seed particles, their activation to cloud droplets and subsequent condensational growth, as well as homogeneous and heterogeneous ice nucleation processes under the prevailing thermodynamic conditions inside LACIS. The main fluid dynamical processes to be considered are fluid flow, and heat and mass transfer. Concerning particle dynamics, transport and phase transitions processes need to

be accounted for. These processes are mathematically described by the momentum, the vapor mass transport, the energy equation and conservation equations for e.g., particle number and mass. The particle dynamical equations account for transport due to convection, diffusion and external forces (thermophoresis, sedimentation), as well as phase transition processes such as condensation/evaporation and homogeneous and heterogeneous ice nucleation. The respective equations are coupled through latent heat release and vapor depletion resulting from the phase transition processes.

To solve the coupled fluid and particle dynamics equations for initial and boundary conditions encountered in LACIS, the Computational Fluid Dynamics code FLUENT (Fluent Inc., 2001) combined with the Fine Particle Model (FPM, particle dynamics GmbH, Wilck et al., 2002; Whitby et al., 2003) are applied. For minimizing computing time, the simulations are realized on a two-dimensional computational grid taking advantage of the system's rotational symmetry.

The fluid momentum equation, assuming steady state conditions, is given by

$$\rho_g(\mathbf{v} \cdot \nabla)\mathbf{v} = -\nabla p + \nabla \cdot (\mu \nabla \mathbf{v}) + \mathbf{V} + \rho_g \mathbf{g} \quad (1)$$

with the density of gas mixture ρ_g , velocity vector \mathbf{v} , pressure p , dynamic viscosity of the vapor-gas mixture μ , the term \mathbf{V} comprising viscosity terms not accounted for in $\nabla \cdot (\mu \nabla \mathbf{v})$, and the vector of gravitational acceleration \mathbf{g} . The vapor mass transport equation has the following form (Bird et al., 1960):

$$\nabla \cdot (\rho_g \mathbf{v} \xi_v) = -\nabla \cdot \mathbf{j}_v + S_v \quad (2)$$

$$\mathbf{j}_v = -\rho_g D_v \nabla \xi_v - \rho_g D_v \alpha_{v,g} (1 - \xi_v) \xi_v \nabla \ln T \quad (3)$$

where ξ_v is the vapor mass fraction, \mathbf{j}_v represents the mass flux of vapor relative to the mass average velocity, S_v specifies the vapor sink due to condensation on particles, droplets or ice particles, D_v is the vapor diffusion coefficient in air and $\alpha_{v,g}$ is the thermal diffusion factor of the vapor-gas mixture. The mass flux of vapor \mathbf{j}_v is governed by two mechanisms, molecular (first term of Eq. 3) and thermal diffusion (second term of Eq. 3).

The energy equation for an air-vapor mixture includes heat transport due to conduction (first term and first part of the second term Eq. 5) and vapor transport accounting for the Dufour effect (second part of second term Eq. 5). This is expressed as

$$\nabla \cdot (\rho_g \mathbf{v} h) = -\nabla \cdot \mathbf{q} + S_h \quad (4)$$

$$\mathbf{q} = -\rho_g \alpha \nabla h - \rho_g (\alpha \nabla \xi_v + \mathbf{j}_v) (h_v - h_g) + \alpha_{v,g} k T \frac{M}{M_v + M_g} \mathbf{j}_v, \quad (5)$$

with the specific enthalpy h , the heat flux \mathbf{q} , heat source S_h , thermal diffusivity $\alpha = k_h / \rho_g c_p$ with heat conductivity k_h and specific heat capacity at constant pressure c_p . h_v and h_g are the specific enthalpies of vapor and gas, M , M_v and M_g represent the molar weights of the mixture, the vapor and the dry

carrier gas, respectively. Hence Eqs. 2 and 4 are coupled via mass transfer due to phase transition processes and resulting release/consumption of energy ($S_h = L_i S_v$ with L_i being either the latent heat of vaporization or fusion) on the one hand and on the other hand due to mass flux of water vapor.

The Modal Aerosol Dynamics method (MAD) (Whitby and McMurry, 1997) is applied to parameterize the particle size distribution. Therefore, the size distribution is split into modes (represented by j) (Whitby and McMurry, 1997; Whitby et al., 2002, 2003), each representing a distinct particle population. Here the following particle populations are distinguished: seed particle-droplet mode ($j = 1$), the homogeneously nucleated ice mode ($j = 2$) and the heterogeneously nucleated ice mode ($j = 3$). Basically two moments $M_{i,j}^k$ (number and mass) are used for representing each mode, i.e., the total particle number concentration N_j ($k = 0$) and the mass concentrations $M_{i,j}$ ($k = 1$), with each chemical component i in the particle being represented by its own mass moment. This corresponds to each mode being internally mixed, monodisperse and moving in size space. From the considered moments, total particle mass and size can be determined for each mode. The moment dynamic equations for the number N_j and mass $M_{i,j}$ concentration for the different modes are given in Table 2 with external particle velocity v , gas velocity v_g , particle diffusion coefficient D_j and the single particle mass $m_{i,j}$ of substance i in mode j . The particle diffusion coefficient is computed via $D_j = \frac{kT C_C}{3\pi v d_p}$, where d_p presents the particle diameter assuming spherical shape and C_C is the Cunningham correction factor, which can be calculated using

$$C_C = 1 + \frac{2\lambda}{d_p} \left(1.257 + 0.4 \exp\left(-0.55 \frac{d_p}{\lambda}\right) \right),$$

where λ specifies the mean free path of the gas molecules. For the description of the dynamic growth of water droplets and ice particles, the single particle growth law according to Barrett and Clement (1988) is used for the droplets and ice particles

$$\frac{\partial m_{i,j}}{\partial t} = \frac{2\pi d_p}{R_v T} \frac{(S_i - S_{i,j})}{\frac{1}{D_{v,i} p_i f_{\text{mass}}} \left(1 - \xi_v \frac{M}{M_{v,i}}\right) + \frac{1}{k_g T f_{\text{heat}}} \left(\frac{L_i}{R_v T}\right)^2}. \quad (6)$$

S_i and $S_{i,j}$ describe the saturation ratios in the gas phase and over the particle surface, whereby Kelvin and Raoult effects (Koehler equation) are accounted for. The equilibrium vapor pressure is given by p_i , f_{mass} and f_{heat} are the mass and heat transfer transition functions, k_g is the carrier gas heat conductivity and L_i represents the latent heat of evaporation and sublimation, respectively. Further quantities in Table 2 are $M_{2,1}$, the mass concentration of liquid water in the seed-particle droplet mode, ρ_g , ρ_w the gas-mixture and liquid water densities, S_{IN} the total surface area of the seed particles' insoluble core ($S_{\text{IN}} = N_0 S_p$). N_0 is the total particle/droplet number and s_p is the surface area of a single particle, and $j_{\text{hom}}(T)$, $j_{\text{het}}(T)$ represent the homogeneous and

heterogeneous nucleation rate coefficient with the units $\text{m}_w^{-3} \text{s}$ and $\text{m}_{\text{SIN}}^{-2} \text{s}$, respectively. The newly-developed phase transition model, which transfers particles from the seed particle-droplet mode to either homogeneous or heterogeneous ice mode, is implemented in the moment dynamics equations via the respective sink/source terms $S_{\text{hom},i}^k$ and $S_{\text{het},i}^k$. These sink/source terms can also be interpreted as freezing rates. $S_{\text{hom},i}^k$ is proportional to the total liquid water volume of the considered droplet population and the temperature dependent homogeneous ice nucleation rate coefficient. Thereby it is assumed that each ice nucleation event leads to an additional frozen droplet of the population. In case the number of ice nucleation events is equal to or exceeds the droplet population number within a time interval the droplet population will freeze instantaneously. $S_{\text{het},i}^k$ is a function of total IN surface area (only insoluble core) and the temperature dependent heterogeneous ice nucleation rate coefficient. Both quantities have the same units: number of nucleation events per unit time and gas volume.

The different modes and the particle fluxes between the modes are illustrated in Fig. 2. In the calculations the seed particles are treated as multicomponent and monodisperse, consisting of an insoluble core (e.g. ATD) and a soluble coating (e.g. $(\text{NH}_4)_2\text{SO}_4$). These particles can be either dry or hygroscopically grown or activated droplets. For the latter two cases liquid water is also a component of the seed particle-droplet mode (left solid line in Fig. 2). The homogeneous and heterogeneous ice modes have the same composition, i.e., they are made up of the insoluble core, the coating and ice. The material properties for the ice phase used for the computations are specified in the Appendix. Through homogeneous ice nucleation, described by the homogeneous freezing rate $S_{\text{hom},i}^k$, particles from the seed particle-droplet mode are transferred to the homogeneous ice mode ($j = 2$). Likewise, the heterogeneous freezing rate $S_{\text{het},i}^k$ determines the transfer to the heterogeneous ice mode ($j = 3$). Consequently, the concept outlined above facilitates the distinction between ice formed via homogeneous and heterogeneous ice nucleation and effects of competing processes can be analyzed. The concept does not depend on any specific homogeneous and/or heterogeneous nucleation rate coefficient, so different coefficients, e.g. those discussed below, can be implemented and tested.

3.2 Ice nucleation rate coefficients

For determining the homogeneous and heterogeneous ice nucleation rate coefficients to be used in FLUENT/FPM, two different model approaches are adopted: (a) Classical Nucleation Theory is applied for both homogeneous and heterogeneous ice nucleation, and (b) CNT is used for modeling homogeneous ice nucleation, but immersion freezing is described by implementing a CNT-based parameterization derived from prior LACIS measurements (Niedermeier et al., 2010).

Table 2. Particle dynamics equations, number concentration N ($k = 0$) and mass concentration M ($k = 1$) in consideration of species i with ammonium sulfate ($i = 1$), liquid water ($i = 2$), ATD ($i = 3$) and ice ($i = 4$) for seed particle-droplet mode ($j = 1$), homogeneous ($j = 2$) and heterogeneous ($j = 3$) ice mode.

	Transport/external forces	Diffusion	Growth Processes	Sink/source term $S_{\text{hom},i}^k$	Sink/source term $S_{\text{het},i}^k$	
$j = 1$						
$k = 0$	N_1	$-\nabla \cdot (\rho_g(\mathbf{v}_g + \mathbf{v})N_1)$	$+\nabla \cdot (\rho_g D_1 \nabla N_1)$	$-\frac{\rho_g}{\rho_w} M_{2,1} j_{\text{hom}}(T)$	$-\rho_g S_{\text{IN}} j_{\text{het}}(T)$	
$k = 1$	M_1	$-\nabla \cdot (\rho_g(\mathbf{v}_g + \mathbf{v})M_{i,1})$	$+\nabla \cdot (\rho_g D_1 \nabla M_{i,1})$	$+N_1 \frac{\partial}{\partial t} M_{i,1}$	$-\left(\frac{M_{i,1}}{N_1}\right) \frac{\rho_g}{\rho_w} M_{2,1} j_{\text{hom}}(T)$	$-\left(\frac{M_{i,1}}{N_1}\right) \rho_g S_{\text{IN}} j_{\text{het}}(T)$
$j = 2$						
$k = 0$	N_2	$-\nabla \cdot (\rho_g(\mathbf{v}_g + \mathbf{v})N_2)$	$+\nabla \cdot (\rho_g D_2 \nabla N_2)$	$+\frac{\rho_g}{\rho_w} M_{2,1} j_{\text{hom}}(T)$		
$k = 1$	M_2	$-\nabla \cdot (\rho_g(\mathbf{v}_g + \mathbf{v})M_{i,2})$	$+\nabla \cdot (\rho_g D_2 \nabla M_{i,2})$	$+N_2 \frac{\partial}{\partial t} M_{i,2}$	$+\left(\frac{M_{i,2}}{N_2}\right) \frac{\rho_g}{\rho_w} M_{2,1} j_{\text{hom}}(T)$	
$j = 3$						
$k = 0$	N_3	$-\nabla \cdot (\rho_g(\mathbf{v}_g + \mathbf{v})N_3)$	$+\nabla \cdot (\rho_g D_3 \nabla N_3)$		$+\rho_g S_{\text{IN}} j_{\text{het}}(T)$	
$k = 1$	M_3	$-\nabla \cdot (\rho_g(\mathbf{v}_g + \mathbf{v})M_{i,3})$	$+\nabla \cdot (\rho_g D_3 \nabla M_{i,3})$	$+N_3 \frac{\partial}{\partial t} M_{i,3}$	$+\left(\frac{M_{i,3}}{N_3}\right) \rho_g S_{\text{IN}} j_{\text{het}}(T)$	

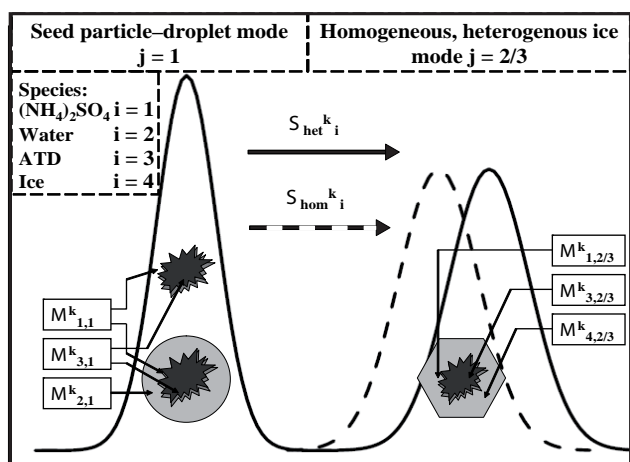


Fig. 2. Schematic of the phase transition in the numerical model with regard of moments (k), modes (j) and species (i) given by integral moments $M_{i,j}^k$. Sink and source term of the seed particle-droplet (solid line), the homogeneous (dashed line) and heterogeneous ice mode (solid line) described by $S_{\text{hom},i}^k$ and $S_{\text{het},i}^k$, respectively. The modes given in this figure are broader for illustration, whereas monodisperse modes are applied in the numerical model.

According to CNT (Pruppacher and Klett, 1997; Seinfeld and Pandis, 1998; Zobrist et al., 2007) the homogeneous nucleation rate coefficient j_{hom} , which is the number of nucleation events per time interval and total liquid water volume of the droplet population, is defined as

$$j_{\text{hom}}(T) = \frac{k_B T}{h} \exp\left(-\frac{\Delta F_{\text{diff}}(T)}{k_B T}\right) N_v \exp\left(-\frac{\Delta G_{\text{hom}}(T)}{k_B T}\right) \quad (7)$$

with the Boltzmann constant k_B , absolute temperature T , Planck constant h , the diffusion energy across the water-ice interface ΔF_{diff} , and the number density of molecules in the bulk water N_v (typical value $3.1 \times 10^{28} \text{ m}^{-3}$, Zobrist et al.,

2007). The critical Gibbs free energy ΔG_{hom} is expressed by

$$\Delta G_{\text{hom}}(T) = \frac{16\pi \sigma_{w/i}^3}{3(n_i(T)k_B T \ln S_{w/i}(T))^2}, \quad (8)$$

where $\sigma_{w/i}$ represents the interfacial free energy of the water-ice boundary, n_i is the number density of molecules in the solid phase and $S_{w/i}$ is the ratio of the saturation vapor pressures over water and ice. The first term of Eq. (7) represents the flux of water molecules to the ice phase and the second term describes the equilibrium number of critical embryos in the liquid phase. Values for quantities such as ΔF_{diff} , $S_{w/i}$ and $\sigma_{w/i}$ are chosen according to Zobrist et al. (2007) and references therein. Altogether the homogeneous nucleation rate coefficient is a very steep function of absolute temperature.

It is known that homogeneous ice nucleation rate coefficients from CNT tend to be too small at temperatures lower than 235 K, but as otherwise good agreement with experiments was found (Jeffery and Austin, 1997; Pruppacher and Klett, 1997; Cantrell and Heymsfield, 2005), they can be used in the temperature range considered here.

Heterogeneous ice nucleation is implemented in the CNT by assuming the insoluble foreign substance, i.e. the IN, increases the likelihood to form a critical embryo, but does not disturb the stochastic nature of the freezing process. So heterogeneous ice nucleation can be derived from the homogeneous case by additionally accounting for the energy barrier reduction due to presence of the IN. Usually this is done based on the concept of contact angle (assuming a spherical cap for ice embryo shape) (Mason, 1971; Pruppacher and Klett, 1997; Seinfeld and Pandis, 1998). The reduced critical Gibbs free energy is then given by

$$\Delta G_{\text{het}}(T) = \Delta G_{\text{hom}} f(\theta), \quad (9)$$

where $f(\theta) = \frac{1}{4}(2 + \cos\theta)(1 - \cos\theta)^2$ is the reduction factor and θ represents the contact angle. θ may vary between 0 and 180°, where the former case implies that the energy barrier is zero (nucleation occurs as soon as supersaturation is reached) and the latter corresponds to homogeneous ice nucleation. The heterogeneous ice nucleation rate coefficient, which is defined as number of nucleation events per time interval and total IN surface, is given by

$$j_{\text{het}}(T) = \frac{k_{\text{B}}T}{h} \exp\left(-\frac{\Delta F_{\text{diff}}(T)}{k_{\text{B}}T}\right) N_{\text{s}} \exp\left(-\frac{\Delta G_{\text{het}}(T)}{k_{\text{B}}T}\right) \quad (10)$$

with the number density of liquid molecules in contact with IN surface N_{s} , which has a typical value of $1 \times 10^{19} \text{ m}^{-2}$.

As a second approach for heterogeneous ice nucleation, a CNT-based parameterization derived from LACIS immersion freezing measurements is implemented into the numerical model. The measurement procedure and the derivation of this CNT-based parameterization are explained in Niedermeier et al. (2010). In principle, this parameterization is a simplified description following CNT, because it captures the essential temperature dependence in a simple way. It is distinguished from the pure CNT approach because a prefactor, which depends on IN surface area and the theoretically uncertain activated complex lifetime and activation energy, is also left as a fitting parameter. Assuming constant temperature and ice nucleation time the heterogeneous ice nucleation rate coefficient $j_{\text{het,LACIS}}(T_{\text{s}})$ is

$$j_{\text{het,LACIS}}(T_{\text{s}}) = \frac{a}{s_{\text{p}}} \exp\left(-C_1 \frac{(1 - \frac{T_{\text{s}}}{C_2})^3}{T_{\text{s}}^2} f_{\text{het}}\right) \quad (11)$$

with a and f_{het} being temperature independent fitting parameters derived from the measured data. The fitting parameter a includes information about the IN surface area of a single particle s_{p} and kinetic effects. f_{het} accounts for IN surface properties, i.e. the influence of the IN surface on thermodynamics. Here $T_{\text{s}} = T_0 - T_{\text{axis}}$ is the supercooling temperature and $C_1 = 5.00 \times 10^5 \text{ K}^2$ and $C_2 = 8.24 \times 10^1 \text{ K}$ are constants resulting from a simplification of the surface free energy and Gibbs free energy terms.

For 300 nm uncoated ATD particles and a ice nucleation time of 1.56 s the fitting parameters have the following values: $a = 1.31 \text{ s}^{-1}$ and $f_{\text{het}} = 4.51 \times 10^{-2}$. This formula is valid over a supercooling range of $235 < T \leq 239 \text{ K}$.

4 Results and discussion

The numerical model FLUENT/FPM as described above is a suitable tool for exploring LACIS' behavior for a given set of boundary conditions, testing assumptions made during the interpretation of experimental data, and evaluating the feasibility of different theoretical approaches for modeling homogeneous and heterogeneous ice nucleation. In the framework of this section, (1) the principle behavior of LACIS when operated in immersion freezing mode will be

described, and (2) experimental data and their interpretation as given in Niedermeier et al. (2010) will be reviewed. In this context, boundary conditions corresponding to those used during the FROST campaign were applied in the numerical simulations. The inlet temperature and the inlet dew point were set to 273.15 K and 265.95 K. The wall temperatures of Sects. 6 and 7 were always identical and varied in a range of $233.15 \leq T_{\text{w},6,7} \leq 240.65 \text{ K}$. Furthermore, the wall boundary condition for sections 6 and 7 was always set to ice saturation ($S_{\text{i}} = 1$), which corresponds to ice covered inner tube walls. For both the homogeneous and the heterogeneous studies the seed particle/IN concentrations were set to 300 cm^{-3} . As each droplet contained a single seed particle/IN this results in a droplet number concentration of 300 cm^{-3} as well. When studying homogeneous and heterogeneous ice nucleation, IN were assumed to be spherical with diameters of 187 or 300 nm, internally mixed consisting of an insoluble ATD core and a small amount (mass fraction of 0.019) of ammonium sulfate. The latter was done to reproduce the activation behavior observed in CCN measurements during the FROST campaign. Concerning ATD, the following material properties were assumed: a molecular weight of 65.18 g mol^{-1} , which is the mass weighted average of the main constituent of ATD and a density of 2600 kg m^{-3} (Möhler et al., 2006).

4.1 Behavior of LACIS operated in immersion mode

In order to study ice nucleation processes in LACIS the thermodynamic conditions such as temperature and saturation with respect to water and ice inside the flow tube have to be known. Due to the coupled heat-vapor diffusion processes taking place, the temperature, vapor concentration and saturation profiles are complex and spatially inhomogeneous. As particles/droplets, to good approximation, are confined to the center of the flow tube, the temperature and saturation profiles at the flow tube centerline are of special interest. Typical profiles of temperature and saturation with respect to water and ice are given as a function of time for different wall temperature settings in Fig. 3. Just the last two tube sections are shown, i.e., the profiles in sections 6 and 7. The temperature profile (Fig. 3, panel 1) exhibits a steep fall within the first freezing section ($t \leq 1.6 \text{ s}$) and approaches the externally-set wall temperatures in the second freezing section ($1.6 \leq t \leq 3.2 \text{ s}$). It should be noted that on average after 2.6 s already, the temperature at the centerline T_{axis} reaches its set value within a range of about $\pm 0.3 \text{ K}$. This range is defined as temperature error in LACIS.

Within the supercooling temperature range ($T < 273.15 \text{ K}$) the vapor pressure over ice is smaller than over supercooled water. Figure 3, panel 2 shows profiles for the saturation with respect to water (solid lines) and ice (dashed lines). For both water and ice the saturation ratio rises strongly until a maximum is reached, then decreases and approaches a constant value. The actual profiles depend on wall temperature and inlet dew point. For constant inlet dew point, the lower the

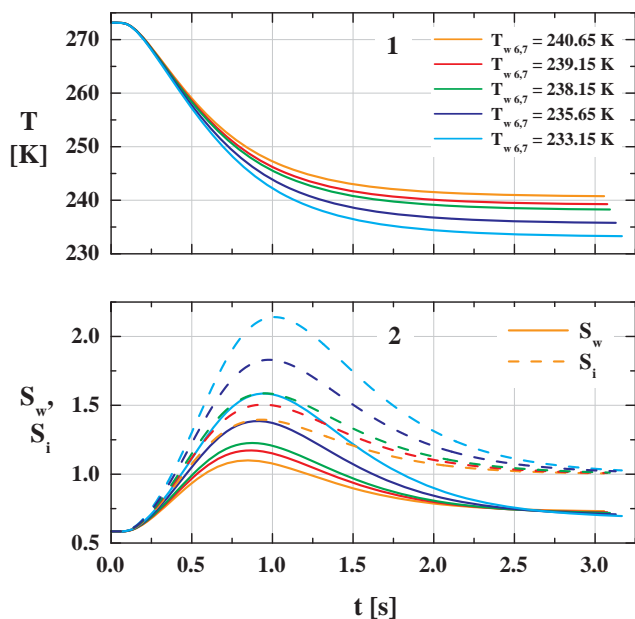


Fig. 3. Profiles at LACIS centerline for different wall temperature settings. Panel 1 shows temperature, panel 2 depicts saturation wrt. water (solid lines) and ice (dashed lines).

wall temperature, the higher are the saturation maxima. At the outlet of LACIS the ice saturation approaches 1, while water saturation converges to a subsaturated level.

The behavior of supercooled water droplets and ice particles under these thermodynamic conditions is explained in Fig. 4, whereas model version (b) in Sect. 3.2 (CNT for modeling homogeneous ice nucleation and CNT-based parameterization for immersion freezing) is applied for forming ice particles. It depicts the mass fractions of water vapor, liquid water and ice as function of time at the centerline of LACIS for a wall temperature of $T_{w,6,7} = 238.15$ K. Here, the mass fractions should be interpreted as total mass of species i (water vapor, liquid water and ice) per total mass of gas. The red line in Fig. 4 represents the water vapor mass fraction, which is defined by the inlet dew point temperature. The mass fraction of water vapor decreases along the centerline of LACIS. Sinks are the flux of water vapor to the inner ice covered tube walls (boundary condition $S_i = 1$), condensation of water vapor on the droplets and deposition of water vapor on the frozen droplets. A mass balance yields that approximately 94% of the water vapor is transported to the ice covered walls. 6% of the inlet water vapor flows out of LACIS and only the remaining small amount on the order of 10^{-5} participates in microphysical processes described in the following. Additionally, for reference the axial temperature T_{axis} is given by the gray curve and the right ordinate.

At first the seed particles grow hygroscopically. As soon as the water saturation increases above the critical super-saturation, the seed particles become activated to liq-

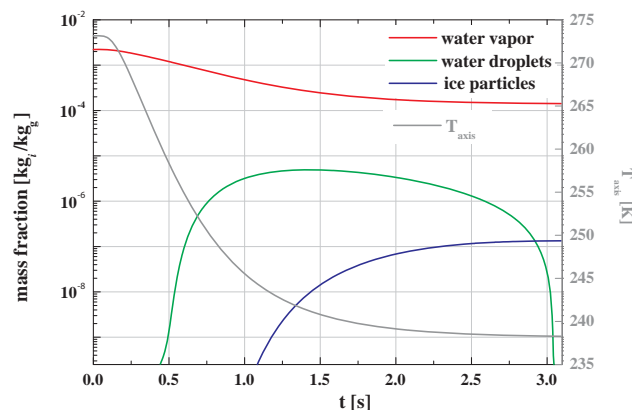


Fig. 4. Mass fraction of water vapor (red line), liquid water (green line) and ice (blue line) at LACIS centerline for $T_{w,6,7} = 238.15$ K (left ordinate). The axial temperature T_{axis} is presented by the gray solid line (right ordinate).

uid droplets, which is seen in Fig. 4 as an increase in the liquid water mass fraction. Subsequently the droplets grow dynamically by vapor diffusion (continuous rise of liquid water mass fraction in Fig. 4) and reach their maximum droplet sizes, which are approx. $2.1 \mu\text{m}$ for $T_{w,6,7} = 240.65$ K, $3.0 \mu\text{m}$ for $T_{w,6,7} = 239.15$ K, $3.5 \mu\text{m}$ for $T_{w,6,7} = 238.15$ K, $4.7 \mu\text{m}$ for $T_{w,6,7} = 235.65$ K and $5.6 \mu\text{m}$ for $T_{w,6,7} = 233.15$ K wall temperature settings. At about $T_{axis} \approx 245$ K ice nucleation starts taking place and the first droplets freeze. Due to further cooling and passage of time, more droplets freeze. The mass fraction of ice particles increases continuously due to more and more droplets freezing and the depositional growth of the already frozen droplets. Figure 4 clearly shows that the droplets are first formed at higher temperatures ($T_{axis} \approx 260$ K) and require further reduction of temperature to freeze. This indicates that for these conditions, immersion freezing is the only freezing process taking place. This supports the observations presented and discussed in Niedermeier et al. (2010), suggesting that immersion freezing is the dominant ice nucleation mechanism. Once water saturation falls below 1 ($T_{axis} \approx 240$ K, $t \approx 1.6$ s) the remaining unfrozen droplets start to evaporate in the ice super- and water subsaturated environment due to the Wegener-Bergeron-Findeisen effect, and evaporate completely before passing the outlet of LACIS. As a result seed particles and different sized ice particles leave the outlet of LACIS. Experimental and theoretical sensitivity studies varying the inlet dew point resulted in dew point temperature ranges to be considered in experimental investigations in which the determined ice fractions are not affected by evaporation of the droplets at too early a stage.

In Fig. 5 the time development of different parameters quantifying homogeneous and heterogeneous ice nucleation are shown. Here homogeneous ice nucleation is calculated according to CNT (Eq. 7). For simulating the

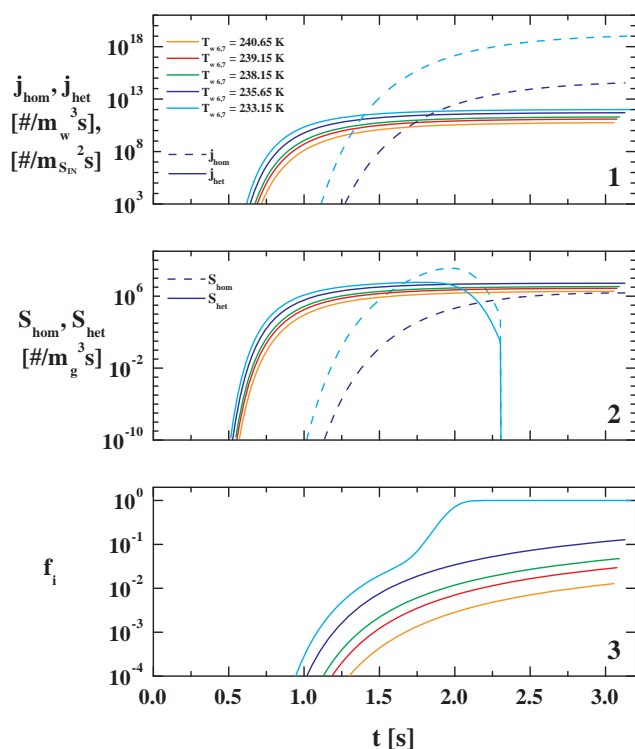


Fig. 5. Ice nucleation parameters for the freezing of supercooled water droplets as function of time along the centerline of LACIS for different wall temperature settings (panel 1: homogeneous (dashed lines) and heterogeneous (solid lines) ice nucleation rate coefficient, panel 2: source term for homogeneous and heterogeneous ice mode, panel 3: resulting ice fraction).

heterogeneous ice nucleation, the immersion freezing parameterization (Eq. 11) derived in Niedermeier et al. (2010) is applied.

Panel 1 illustrates the homogeneous j_{hom} and heterogeneous j_{het} ice nucleation rate coefficients. First of all j_{het} rises steeply and approaches a nearly constant value ($t > 1.5$ s corresponds to the beginning of Sect. 7 in which the absolute temperature T is nearly constant). j_{hom} increases later and at lower temperatures compared to j_{het} . It is only non-negligible for the wall temperature settings of $T_{w,6,7} = 335.65$ K and $T_{w,6,7} = 333.15$ K. But it should be noted that homogeneous and heterogeneous ice nucleation rate coefficients, because of their different dimensions ($[j_{\text{hom}}] = \text{m}_w^{-3}\text{s}$ and $[j_{\text{het}}] = \text{m}_{\text{SIN}}^{-2}\text{s}$), can only be compared qualitatively. For quantitative comparison, freezing rates for homogeneous S_{hom} and heterogeneous ice nucleation S_{het} (illustrated in panel 2) are more appropriate, as these quantities feature the same dimensions. S_{het} has a similar shape compared to j_{het} . S_{hom} increases at lower temperatures than S_{het} and is smaller than S_{het} except at $T_{w,6,7} = 333.15$ K. This implies that first, ice formation takes place via heterogeneous ice nucleation, and only if S_{hom} becomes effective (for $T_{w,6,7} \leq 335.65$ K) ice is also formed due to homogeneous

ice nucleation. For $T_{w,6,7} = 333.15$ K, both the homogeneous and the heterogeneous source terms drop to zero at $t = 2.3$ s, as all supercooled water droplets have been frozen. This can also be seen in panel 3 depicting the ice fraction f_i , which is the ratio of ice particle number N_i per total particle number N_0 . At sufficiently low temperatures ($T \approx 243.5$ K) immersion freezing takes place and the ice fraction exceeds the experimental detection limit of 10^{-4} . The ice fraction f_i increases monotonically with decreasing temperature, and for $T_{w,6,7} = 333.15$ K, f_i rises steeply when homogeneous ice nucleation sets in and becomes dominant. In general the lower the wall temperature the higher the ice fraction.

Summing up the results of the numerical simulations discussed in this section, it can be stated that over the experimental parameter space (wall temperatures, dew points, residence times, etc.) investigated, ice nucleation is clearly dominated by immersion freezing for all cases apart from $T_{w,6,7} = 333.15$ K, where homogeneous ice nucleation becomes dominant at about 234.9 K. Homogeneous freezing is negligible for $T_{w,6,7} > 235.65$ K. The ice nucleation time varies in a range of 1.7 to 2.1 s for the respective wall temperature settings and the vast bulk of ice is formed in Sect. 7, where the temperature is almost constant.

4.2 Comparison of experiments and model simulations

The numerical model can also be used to interpret experimental data collected with LACIS: e.g. understanding the relative importance of processes involved, evaluating the feasibility of different theoretical approaches, and checking the validity of assumptions made. Specifically, here the relative importance of homogeneous vs. heterogeneous ice nucleation during immersion freezing experiments at LACIS, the applicability of CNT to describe the immersion freezing behavior of ATD particles, and the feasibility of assuming a constant temperature when deriving parameterizations for ice nucleation rate coefficients from LACIS-measured ice fractions, will be explored.

Figure 6 shows a comparison of ice fractions as measured with LACIS and calculated with FLUENT/FPM, as a function of temperature. The experimental data are represented by the orange (ice fractions as measured for 300 nm ATD particles) and the black (ice fractions determined for highly diluted ammonium sulfate solution droplets) squares. Concerning the model simulations, results applying homogeneous (solid line, Eq. 7) and heterogeneous (broken lines, Eq. 10) CNT are given. The temperature on the x-axis corresponds to the wall temperatures of sections 6 and 7 ($T_{w,6,7}$).

Looking at the experimental data in Fig. 6, it becomes obvious that, when considering ATD particles as IN, around $T = 236$ K the slope of the f_i vs. temperature curve becomes steeper. A similar behavior can be found considering the ice fractions measured for the highly diluted solution droplets. Now comparing theoretical and experimental results, it can be seen that homogeneous nucleation theory according to

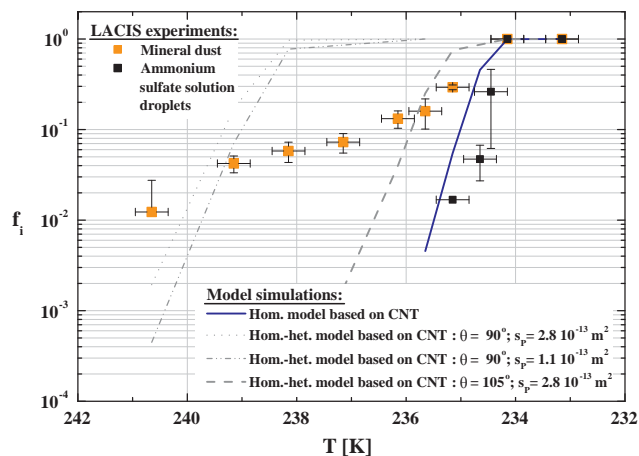


Fig. 6. Comparison of LACIS experiments (freezing of droplets containing 300 nm mineral dust particles acting as IN: orange cubes and freezing of highly dilutes ammonium sulfate solution droplets: black cubes) with Fluent/FPM model simulation results. The blue curve presents homogeneous ice nucleation according to CNT. Model simulations taking both freezing modes into account, homogeneous and heterogeneous, based on CNT are given for different contact angles and total IN surfaces ($\theta = 90^\circ$, $s_p = 2.8 \cdot 10^{-13} \text{ m}^2$: grey dashed-dotted curve; $\theta = 90^\circ$, $s_p = 1.1 \cdot 10^{-13} \text{ m}^2$: grey dotted curve; $\theta = 105^\circ$, $s_p = 2.8 \cdot 10^{-13} \text{ m}^2$: grey dashed curve).

CNT (solid line) is able to explain the behavior of the ammonium sulfate solution droplets (both slope and absolute values are predicted with reasonable accuracy). However, heterogeneous nucleation theory according to CNT, assuming constant contact angles (model version (a)), fails to predict the observed freezing behavior. Neither the ice fractions, nor the slope of the ice fraction vs. temperature curve match (the predicted slope is much steeper), regardless of the actual contact angle. Furthermore, it can be seen that decreasing the total particle surface area by a factor of 2.6 (dotted curve compared to dashed-dotted-dotted curve), the ice fraction decreases slightly, but the shape of the curve remains almost constant.

Interpreting these results the following statements can be made for the experimental parameter space considered here: Classical homogeneous ice nucleation theory, utilizing the properties as given in Zobrist et al. (2007), is able to predict the freezing behavior of highly diluted ammonium sulfate solution droplets. Classical heterogeneous ice nucleation theory together with the assumption of constant contact angle fails to predict the experimental observations made of the immersion freezing behavior of ATD particles.

Investigating immersion freezing of water droplets coated with a nonadecanol monolayer and deducing the heterogeneous ice nucleation rate coefficients from these measurements, Zobrist et al. (2007) found similar results. The CNT model using constant contact angle cannot reproduce those measurements because the slope of the j_{het} curve is too steep.

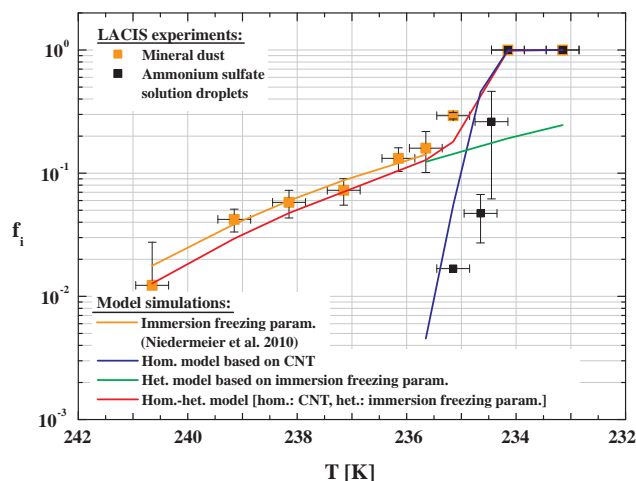


Fig. 7. Comparison of LACIS experiments (freezing of droplets containing 300 nm mineral dust particles acting as IN: orange cubes and freezing of highly dilutes ammonium sulfate solution droplets: black cubes) with Fluent/FPM model simulation results. The orange line represents the immersion freezing parameterization derived in Niedermeier et al. (2010). The model simulations applying either homogeneous ice nucleation according to CNT (blue line), or heterogeneous ice nucleation based on the immersion freezing parameterization derived in Niedermeier et al. (2010) (green line) or the combination of both (red line).

As a result Zobrist et al. (2007) assume a linear temperature dependence of the contact angle in order to get their experimental results and theory into agreement. Marcolli et al. (2007) analyzed the immersion freezing behavior of droplets containing several distinct sized ATD particles with differential scanning calorimeter technique. They also stated, that a regular stochastic model (CNT) cannot explain their experimental results. Simulations assuming a stochastic-singular model with contact angle distribution (singular model following the authors terminology), where the contact angles vary between the particles considered, or accounting for a distribution of active sites led also to better agreement. Similar conclusions concerning the insufficiency of a constant contact angle model describing experiments accurately were drawn in Lüönd et al. (2010), where the immersion freezing behavior of size-selected kaolinite particles was studied.

In Niedermeier et al. (2010) an alternative approach to Zobrist et al. (2007) and Marcolli et al. (2007) for parameterizing experimental results based on CNT was suggested (Eq. 11). Validity of the assumptions made in this context will be discussed in the following.

Similar to Fig. 6, Fig. 7 depicts ice fractions as a function of temperature with the experimental data (orange and black squares) being identical. The orange solid line represents results from the CNT-based parameterization as given in Niedermeier et al. (2010), i.e. Eq. (11) is used for calculating the ice fractions. The other solid lines correspond to results

from FLUENT/FPM with different assumptions for calculating the freezing rate. Shown are results determined assuming just homogeneous (blue line), just heterogeneous (green line), and both homogeneous and heterogeneous (red line, corresponds to model version (b) in Sect. 3.2) ice nucleation being active. The latter curve compares well with the experimental data, indicating that the FLUENT/FPM is a suitable tool for describing the complex fluid/particle dynamical and phase transition processes taking place in LACIS. The results from the model simulations taking either homogeneous (blue line) or heterogeneous (green line, underlying the red curve for $T > 235.65$ K) ice nucleation into account show clearly that immersion freezing is dominant for $T > 234.9$ K, while at lower temperatures homogeneous freezing is the main process. It should be noted that in the parameter space investigated here, heterogeneous ice nucleation is not quenching homogeneous ice nucleation. In other words, even for a reasonably effective IN such as pure ATD, there is a temperature range in which either both mechanisms can be active or even homogeneous nucleation can be dominant, although every supercooled droplet has a particle immersed. The main reason is the apparently different temperature dependence of the two freezing mechanisms. The actual explanation of why the two mechanisms feature different temperature dependencies remains the topic of future investigations.

Now concentrating on the temperature range in which immersion freezing is dominant and comparing the orange to the green line (underlying the red one in the range of interest) it can be seen that the green line, corresponding to the FLUENT/FPM results, is slightly lower, however still within the level of uncertainty of the experimental data, than the orange one representing data generated with the CNT-based parameterization given in Niedermeier et al. (2010). This parameterization was determined assuming the temperature to be constant during the ice nucleation process and equal to the wall temperature of the last tube section. The time period where the temperature at the centerline is almost constant (deviation $+0.3$ K) was taken as ice nucleation time. In contrast, the FLUENT/FPM simulations, even though being based on the same nucleation rate coefficient, account for the detailed temperature variation along the flow tube center line (Fig. 7). The small difference between the two data sets is indicative that the assumptions made in Niedermeier et al. (2010) concerning both nucleation temperature and ice nucleation time are justified. Consequently, the method assuming constant temperature during ice nucleation and the chosen nucleation time for determining the fitting coefficients in the CNT-based parameterization equation are justified and valid. For verifying the parameterization concept itself, further investigations analyzing the immersion freezing behavior as function of temperature (wider temperature range than investigated in the present paper), IN surface (varying ice nucleus sizes), IN structure and chemical composition and ice nucleation time are fundamentally necessary.

5 Summary and conclusions

Homogeneous and heterogeneous ice nucleation, in particular the immersion freezing of Arizona Test Dust (ATD) particles, have been studied both theoretically and experimentally with the Leipzig Cloud Interaction Simulator (LACIS). In the framework of the present paper, both the physical LACIS setup as used e.g. during the two FROST measurement campaigns (see also Niedermeier et al., 2010; Sullivan et al., 2010; Reitz et al., 2011; Wex et al., 2011), and the numerical model developed to design experiments and interpret their results have been presented in detail. The model developed and used for the theoretical investigations is based on the commercially available computational fluid dynamics code FLUENT and the Fine Particle Model (FPM). Both together allow for the coupled solution of the conservation equations for momentum, mass, heat and seed particle, droplet, ice particle number and mass, needed to describe the complex fluid/particle dynamical and phase transition processes taking place inside LACIS. Using this model, the operating principle of LACIS has been presented, (a) outlining its ability to perform both homogeneous and heterogeneous freezing (specifically immersion freezing) experiments, and (b) defining the experimental parameter space (temperatures, dew points, seed particle number concentrations, etc.) in which such experiments can be performed.

For the evaluation of different model approaches for the description of homogeneous and heterogeneous ice nucleation, model simulations were carried out applying Classical Nucleation Theory (CNT) for homogeneous and heterogeneous ice nucleation. Concerning the latter, a constant contact angle was assumed. It was found that for the experimental parameter space considered, classical homogeneous nucleation theory, utilizing the properties as given in Zobrist et al. (2007), is able to predict the freezing behavior of highly diluted ammonium sulfate solution droplets. However, classical heterogeneous nucleation theory, together with the assumption of a constant contact angle, fails to predict the experimental observations made concerning the immersion freezing behavior of ATD particles. The main reason for this failure is the apparently too strong temperature dependence of the nucleation rate coefficient.

Assuming CNT for homogeneous ice nucleation and the CNT-based parameterization according to Niedermeier et al. (2010) for heterogeneous ice nucleation, it was found that the simulated freezing behavior was in good agreement with the measured values. Also, it was found that in the experimental parameter space investigated, heterogeneous ice nucleation is not necessarily quenching homogeneous ice nucleation. Even for a reasonably effective IN such as pure ATD there are temperature regimes where homogeneous ice nucleation is dominant. The main reason are the different temperature dependencies of the two freezing mechanisms.

Finally, reviewing the assumptions concerning constant temperature and ice nucleation time made in Niedermeier

et al. (2010) when deriving a CNT-based parameterization for the nucleation rate coefficient in the immersion freezing mode, the good agreement between parameterization and simulation results shows that both assumptions were justified. This underlines the applicability of the method to determine the fitting coefficients in the CNT-based parameterization equation.

Appendix A

To describe the material ice in the numerical model following temperature dependent properties are required: density, heat capacity at constant pressure, interfacial free energy between ice and vapor phase, latent heat of sublimation, thermal conductivity and vapor pressure. For the ice density ρ_i the parameterization in Pruppacher and Klett (1997) is applied:

$$\rho_i(T) = 916.7 - 0.175T - 0.0005T^2 \quad (\text{A1})$$

with T in K and ρ_i in kg m^{-3} . Heat capacity values of ice are given by Giaque and Stout (1936) in a temperature range of $15 < T < 273$ K in the unit $\text{J mol}^{-1} \text{K}^{-1}$:

$$c_p(T) = 104.54 + 7.3245T. \quad (\text{A2})$$

The experimentally determined interfacial free energy

$$\sigma_{w/i} = 0.109 \frac{\text{N}}{\text{m}} = \text{const.} \quad (\text{A3})$$

according to Ketcham and Hobbs (1969) is used for the simulations. The latent heat of fusion L_f is derived from experiments of Murphy and Koop (2005):

$$L_f = 47425.017 + 31.053 \cdot T - 0.065 \cdot T^2 \quad (\text{A4})$$

with L_f in J mol^{-1} . The vapor pressure over ice is approximated by the equation of Goff and Gratch¹.

Acknowledgements. The measurement campaign FROST was conducted within the Helmholtz Virtual Institute ‘‘Aerosol-Cloud Interactions’’ funded by the Helmholtz society. This work is part of a DFG project under contract HE 939/21-1. Additionally, the campaign was financially supported by the research project EUROCHAMP funded within the EC 6th Framework Program, Section ‘‘Support for Research Infrastructures – Integrated Infrastructure Initiative’’. RAS acknowledges support from the Alexander von Humboldt Foundation during the time this research was carried out.

Edited by: R. Krejci

References

- Barrett, J. C. and Clement, C. F.: Growth-Rates For Liquid-Drops, *J. Aerosol Sci.*, 19, 223–242, 1988.
- Bird, R., Stewart, W., and Lightfoot, E.: *Transport Phenomena*, John Wiley, 780 pp., 1960.
- Bundke, U., Nillius, B., Jaenicke, R., Wetter, T., Klein, H., and Bingemer, H.: The fast Ice Nucleus chamber FINCH, *Atmos. Res.*, 90, 180–186, doi:10.1016/j.atmosres.2008.02.008, 2008.
- Cantrell, W. and Heymsfield, A.: Production of ice in tropospheric clouds – a review, *B. Am. Meteorol. Soc.*, 86(6), 795–807, 2005.
- Chang, H. Y. A., Koop, T., Molina, L. T., and Molina, M. J.: Phase transitions in emulsified $\text{HNO}_3/\text{H}_2\text{O}$ and $\text{HNO}_3/\text{H}_2\text{SO}_4/\text{H}_2\text{O}$ solutions, *J. Phys. Chem. A*, 103, 2673–2679, 1999.
- Cziczo, D. J., Murphy, D. M., Hudson, P. K., and Thomson, D. S.: Single particle measurements of the chemical composition of cirrus ice residue during crystal-face, *J. Geophys. Res.-Atmos.*, 109, D04201, doi:10.1029/2003JD004032, 2004.
- Davis, E. J.: A history of single aerosol particle levitation, *Aerosol Sci. Technol.*, 26, 212–254, 1997.
- DeMott, P. J., Cziczo, D. J., Prenni, A. J., Murphy, D. M., Kreidenweis, S. M., Thomson, D. S., Borys, R., and Rogers, D. C.: Measurements of the concentration and composition of nuclei for cirrus formation, *Proc. Natl. Acad. Sci. USA*, 100(25), 14655–14660, 2003a.
- DeMott, P. J., Sassen, K., Poellot, M. R., Baumgardner, D., Rogers, D. C., Brooks, S. D., Prenni, A. J., and Kreidenweis, S. M.: African dust aerosols as atmospheric ice nuclei, *Geophys. Res. Lett.*, 30(14), 1732, doi:10.1029/2003GL017410, 2003b.
- Diehl, K. and Mitra, S. K.: A laboratory study of the effects of a kerosene-burner exhaust on ice nucleation and the evaporation rate of ice crystals, *Atmos. Environ.*, 32, 3145–3151, 1998.
- Duft, D. and Leisner, T.: Laboratory evidence for volume-dominated nucleation of ice in supercooled water microdroplets, *Atmos. Chem. Phys.*, 4, 1997–2000, doi:10.5194/acp-4-1997-2004, 2004.
- Durant, A. J. and Shaw, R. A.: Evaporation freezing by contact nucleation inside-out, *Geophys. Res. Lett.*, 32, L20814, doi:10.1029/2005GL024175, 2005.
- FLUENT: FLUENT 6 user’s guide, FLUENT Inc., available online at: http://combust.hit.edu.cn:8080/fluent/Fluent60_help/html/ug/main_pre.htm, 2001.
- Giaque, W. F. and Stout, J. W.: The Entropy of Water and the Third Law of Thermodynamics, The Heat Capacity of Ice from 15 to 273 Degree Kelvin, *J. Am. Chem. Soc.*, 58, 1144–1150, doi:10.1021/ja01298a023, 1936.
- Hirst, E., Kaye, P. H., Greenaway, R. S., Field, P., and Johnson, D. W.: Discrimination of micrometre-sized ice and supercooled droplets in mixed-phase cloud, *Atmos. Environ.*, 35, 33–47, 2001.
- Hung, H. M., Malinowski, A., and Martin, S. T.: Kinetics of heterogeneous ice nucleation on the surfaces of mineral dust cores inserted into aqueous ammonium sulfate particles, *J. Phys. Chem. A*, 107(9), 1296–1306, 2003.
- Jeffery, C. A. and Austin, P. H.: Homogeneous nucleation of supercooled water: Results from a new equation of state, *J. Geophys. Res.-Atmos.*, 102, 25269–25279, 1997.
- Kärcher, B. and Lohmann, U.: A parameterization of cirrus cloud formation: Heterogeneous freezing, *J. Geophys. Res.-Atmos.*, 108, 4402, doi:10.1029/2002JD003220, 2003.

¹<http://cires.colorado.edu/~voemel/vp.html>

- Ketcham, W. M. and Hobbs, P. V.: An Experimental Determination Of Surface Energies Of Ice, *Philosoph. Mag.*, 19, 1161–1173, 1969.
- Kiselev, A., Wex, H., Stratmann, F., Nadeev, A., and Karpushenko, D.: White-light optical particle spectrometer for in situ measurements of condensational growth of aerosol particles, *Appl. Optics*, 44, 4693–4701, 2005.
- Knutson, E. O. and Whitby, K. T.: Aerosol classification by electric mobility: Apparatus, theory and applications, *J. Aerosol Sci.*, 6, 443–451, 1975.
- Koop, T., Ng, H. P., Molina, L. T., and Molina, M. J.: A new optical technique to study aerosol phase transitions: The nucleation of ice from H₂SO₄ aerosols, *J. Phys. Chem. A*, 102, 8924–8931, 1998.
- Koop, T., Bertram, A. K., Molina, L. T., and Molina, M. J.: Phase transitions in aqueous NH₄HSO₄ solutions, *J. Phys. Chem. A*, 103, 9042–9048, 1999.
- Lohmann, U.: Aerosol effects on clouds and climate, *Space Sci. Rev.*, 125, 129–137, doi:10.1007/s11214-006-9051-8, 2006.
- Lüönd, F., Stetzer, O., Welti, A., and Lohmann, U.: Experimental study on the ice nucleation ability of size-selected kaolinite particles in the immersion mode, *J. Geophys. Res.*, 115, D14201, doi:10.1029/2009JD012959, 2010.
- Marcotilli, C., Gedamke, S., Peter, T., and Zobrist, B.: Efficiency of immersion mode ice nucleation on surrogates of mineral dust, *Atmos. Chem. Phys.*, 7, 5081–5091, doi:10.5194/acp-7-5081-2007, 2007.
- Mason, B. J.: *The Physics of Clouds*, 2nd ed., Clarendon Press, 1971.
- Möhler, O., Stetzer, O., Schaefer, S., Linke, C., Schnaiter, M., Tiede, R., Saathoff, H., Krämer, M., Mangold, A., Budz, P., Zink, P., Schreiner, J., Mauersberger, K., Haag, W., Kärcher, B., and Schurath, U.: Experimental investigation of homogeneous freezing of sulphuric acid particles in the aerosol chamber AIDA, *Atmos. Chem. Phys.*, 3, 211–223, doi:10.5194/acp-3-211-2003, 2003.
- Möhler, O., Field, P. R., Connolly, P., Benz, S., Saathoff, H., Schnaiter, M., Wagner, R., Cotton, R., Krämer, M., Mangold, A., and Heymsfield, A. J.: Efficiency of the deposition mode ice nucleation on mineral dust particles, *Atmos. Chem. Phys.*, 6, 3007–3021, doi:10.5194/acp-6-3007-2006, 2006.
- Murphy, D. M. and Koop, T.: Review of the vapour pressures of ice and supercooled water for atmospheric applications, *Q. J. Roy Meteor. Soc.*, 131, 1539–1565, 2005.
- Murray, B. J., Broadley, S. L., Wilson, T. W., Bull, S. J., Wills, R. H., Christenson, H. K., and Murray, E. J.: Kinetics of the homogeneous freezing of water, *Phys. Chem. Chem. Phys.*, 12, 10380–10387, doi:10.1039/c003297b, 2010.
- Niedermeier, D., Wex, H., Voigtländer, J., Stratmann, F., Brüggemann, E., Kiselev, A., Henk, H., and Heintzenberg, J.: LACIS-measurements and parameterization of sea-salt particle hygroscopic growth and activation, *Atmos. Chem. Phys.*, 8, 579–590, doi:10.5194/acp-8-579-2008, 2008.
- Niedermeier, D., Hartmann, S., Shaw, R. A., Covert, D., Mentel, T. F., Schneider, J., Poulain, L., Reitz, P., Spindler, C., Clauss, T., Kiselev, A., Hallbauer, E., Wex, H., Miltenberger, K., and Stratmann, F.: Heterogeneous freezing of droplets with immersed mineral dust particles - measurements and parameterization, *Atmos. Chem. Phys.*, 10, 3601–3614, doi:10.5194/acp-10-3601-2010, 2010.
- Particle Dynamics: FPM User's Guide, available at: www.particle-dynamics.de, Particle Dynamics GmbH, Leipzig, Germany, 2005.
- Prospero, J. M.: Long-term measurements of the transport of African mineral dust to the southeastern United States: Implications for regional air quality, *J. Geophys. Res.-Atmos.*, 104(D13), 15917–15927, 1999.
- Pruppacher, H. R. and Klett, J. D.: *Microphysics of Clouds and Precipitation*, Kluwer Academic Publishers, Dordrecht, The Netherlands, 78–99, 192–215 and 341–354, 1997.
- Pruppacher, H. R. and Neuberger, M.: Design and performance of the UCLA cloud tunnel. Proceedings of the International Conference on Cloud Physics, Toronto, Canada, 389–392, 1968.
- Reischl, G. P.: The relationship of input and output aerosol characteristics for an ideal differential mobility analyzer particle standard, *J. Aerosol Sci.*, 22, 297–312, 1991.
- Reitz, P., Spindler, C., Mentel, T. F., Poulain, L., Wex, H., Miltenberger, K., Niedermeier, D., Hartmann, S., Clauss, T., Stratmann, F., Sullivan, R., DeMott, P. J., Petters, M. D., Sierau, B., and Schneider, J.: Surface modification of mineral dust particles by sulphuric acid processing: Implications for CCN and IN abilities, *Atmos. Chem. Phys. Discuss.*, submitted, 2001.
- Richardson, M. S., DeMott, P. J., Kreidenweis, S. M., Cziczo, D. J., Dunlea, E. J., Jimenez, J. L., Thomson, D. S., Ashbaugh, L. L., Borys, R. D., Westphal, D. L., Casuccio, G. S., and Lersch, T. L.: Measurements of heterogeneous ice nuclei in the western United States in springtime and their relation to aerosol characteristics, *J. Geophys. Res.-Atmos.*, 112, D02209, doi:10.1029/2006JD007500, 2007.
- Rogers, D. C.: Development of a Continuous Flow Thermal Gradient Diffusion Chamber for Ice Nucleation Studies, *Atmos. Res.*, 22, 149–181, 1988.
- Sassen, K., DeMott, P. J., Prospero, J. M., and Poellot, M. R.: Saharan dust storms and indirect aerosol effects on clouds: Crystal-face results, *Geophys. Res. Lett.*, 30, 1633, doi:10.1029/2003GL017371, 2003.
- Seifert, P., Ansmann, A., Mattis, I., Wandinger, U., Tesche, M., Engelmann, R., Müller, D., Perez, C. and Hausteiner, K.: Saharan dust and heterogeneous ice formation: Eleven years of cloud observations at a central European EARLINET site, *J. Geophys. Res.-Atmos.*, 115(13), D20201, doi:10.1029/2009JD013222, 2010.
- Seinfeld, J. and Pandis, S.: *Atmospheric Chemistry and Physics From Air Pollution to Climate Change*, Wiley-Interscience, Seinfeld, J. H. and Pandis, S. N.: *Atmospheric Chemistry and Physics From Air Pollution to Climate Change*. Wiley Interscience, 556–591, 1998.
- Shaw, R. A., Durant, A. J., and Mi, Y.: Heterogeneous surface crystallization observed in undercooled water, *J. Phys. Chem. B*, 109, 9865–9868, 2005.
- Stetzer, O., Baschek, B., Luond, F., and Lohmann, U.: The Zurich Ice Nucleation Chamber (ZINC) – A new instrument to investigate atmospheric ice formation, *Aerosol Sci. Technol.*, 42, 64–74, doi:10.1080/02786820701787944, 2008.
- Stratmann, F., Kiselev, A., Würzler, S., Wendisch, M., Heintzenberg, J., Charlson, R. J., Diehl, K., Wex, H., and Schmidt, S.: Laboratory studies and numerical simulations of cloud droplet formation under realistic supersaturation conditions, *J. Atmos.*

- Ocean. Tech., 21(6), 876–887, 2004.
- Sullivan, R. C., Petters, M. D., DeMott, P. J., Kreidenweis, S. M., Wex, H., Niedermeier, D., Hartmann, S., Clauss, T., Stratmann, F., Reitz, P., Schneider, J., and Sierau, B.: Irreversible loss of ice nucleation active sites in mineral dust particles caused by sulphuric acid condensation, *Atmos. Chem. Phys.*, 10, 11471–11487, doi:10.5194/acp-10-11471-2010, 2010.
- Takahashi, T.: Riming electrification as a charge generation mechanism in thunderstorms, *J. Atmos. Sci.*, 35, 1536–1548, 1978.
- Voigtländer, J., Stratmann, F., Niedermeier, D., Wex, H., and Kiselev, A.: Mass accommodation coefficient of water: A combined computational fluid dynamics and experimental data analysis, *J. Geophys. Res.*, 112, D20208, doi:10.1029/2007JD008604, 2007.
- Wex, H., Kiselev, A., Ziese, M., and Stratmann, F.: Calibration of LACIS as a CCN detector and its use in measuring activation and hygroscopic growth of atmospheric aerosol particles, *Atmos. Chem. Phys.*, 6, 4519–4527, doi:10.5194/acp-6-4519-2006, 2006.
- Wex, H., Hennig, T., Salma, I., Ocskay, R., Kiselev, A., Henning, S., Massling, A., Wiedensohler, A., and Stratmann, F.: Hygroscopic growth and measured and modeled critical super-saturations of an atmospheric HULIS sample, *Geophys. Res. Lett.*, 34, L02818, doi:10.1029/2006GL028260, 2007.
- Wex, H., Clauss, T., Covert, D., Hallbauer, E., Hartmann, S., Kiselev, A., Mentel, T. F., Mildner, K., Niedermeier, D., Poulain, L., Reitz, P., Schneider, J., Shaw, R., Spindler, C., and Stratmann, F.: Classifying coated and uncoated arizona test dust with respect to hygroscopic growth and activation, *Atmos. Chem. Phys. Discuss.*, in preparation, 2011.
- Whitby, E., Stratmann, F., and Wilck, M.: Fine Particle model (FPM) for FLUENT, Manual, online available at: see: www.particle-dynamics.de, 2003.
- Whitby, E., Stratmann, F., and Wilck, M.: Merging and remapping modes in modal aerosol dynamics models: a “Dynamic Mode Manager”, *J. Aerosol Sci.*, 33, 623–645, 2002.
- Whitby, E. R. and McMurry, P. H.: Modal aerosol dynamics modeling, *Aerosol Sci. Technol.*, 27, 673–688, 1997.
- Wilck, M., Stratmann, F., and Whitby, E. R.: A fine particle model for FLUENT: Description and application, Proc. Sixth Int. Aerosol Conf., Taipei, Taiwan, Chinese Association for Aerosol Research in Taiwan/International Aerosol Research Assembly, 1269–1270, 2002.
- Ziese, M., Wex, H., Nilsson, E., Salma, I., Ocskay, R., Hennig, T., Massling, A., and Stratmann, F.: Hygroscopic growth and activation of HULIS particles: experimental data and a new iterative parameterization scheme for complex aerosol particles, *Atmos. Chem. Phys.*, 8, 1855–1866, doi:10.5194/acp-8-1855-2008, 2008.
- Zobrist, B., Koop, T., Luo, B. P., Marcolli, C., and Peter, T.: Heterogeneous ice nucleation rate coefficient of water droplets coated by a nonadecanol monolayer, *J. Phys. Chem. C*, 111(5), 2149–2155, 2007.
- Zuberi, B., Bertram, A. K., Cassa, C. A., Molina, L. T., and Molina, M. J.: Heterogeneous nucleation of ice in $(\text{NH}_4)_2\text{SO}_4\text{-H}_2\text{O}$ particles with mineral dust immersions, *Geophys. Res. Lett.*, 29(10), 1504, doi:10.1029/2001GL014289, 2002.